Dyes and Pigments 222 (2024) 111844

Contents lists available at ScienceDirect

Dyes and Pigments

journal homepage: www.elsevier.com/locate/dyepig

Phenanthrolines decorated with branched lipophilic chains and their yellow emitting heteroleptic iridium(III) complexes: Synthesis, photophysical and acidochromic behaviour, and computational analysis

Ana M. Garrote Cañas [a], Xue Yong [b], Maha S. Alenezi [c], Natalia Martsinovich [b], Natalia N. Sergeeva [a,d,*]

[a] School of Design, University of Leeds, Leeds, LS2 9JT, UK
[b] Department of Chemistry, University of Sheffield, Sheffield, S3 7HF, UK
[c] Department of Chemistry, Faculty of Arts and Science, Northern Border University, Rafha, Saudi Arabia
[d] Leeds Institute of Textiles and Colour (LITAC), University of Leeds, Leeds, LS2 9JT, UK

ARTICLE INFO

Keywords:
Phenanthroline
Photoluminescence
Computational modelling
Heteroleptic iridium(III) complexes
Acidochromism
Lipophilic chains

ABSTRACT

To improve the solubility and to manipulate the optical properties of phenanthroline-based materials, a series of compounds with branched lipophilic chains Phen1-4 was prepared in three steps with the yield of 22–81%. In addition, a related phenanthroline-based bidental compound Phen5 was synthesised with blocked *N* sites on imidazolyl units to influence π-π* and n-π* transitions and to increase F_{PL}. The optical properties were analysed by UV–vis absorption and fluorescence spectroscopy, showing a strong emission at 427–437 nm and improved F_{PL} for the series (20–68%). Furthermore, Phen2-4 and bidental Phen5 exhibited a clear acidochromic behaviour with a dramatic shift in absorption spectra of ca. 30 nm achieved after the addition of 1 eq. and 2 eq. of an acid (TFA), respectively. Likewise, all compounds showed a loss of fluorescence under acidic conditions. Next, to test the complexation ability of these ligands, the heteroleptic iridium(III) complexes Ir1-4 were prepared in excellent yields (86–98%), along with the binuclear complex Ir5. Their optical properties revealed strong yellow emission centered at 539–571 nm with F_{PL} of up to 7%; additionally, all complexes exhibited large Stokes shifts (220–290 nm).

1. Introduction

For decades, 1,10-phenanthroline (Phen) has been used as a versatile starting material in organic, inorganic and supramolecular chemistry [1]. It has appealing chemical and structural properties, such as aromaticity, basicity, coplanarity, rigidity and chelating capability (two nitrogen atoms in juxtaposition) [1,2]. These properties have been exploited in biomedical screening and sensing [3–5], PDT [6,7], and cancer therapy [8], to name a few. Furthermore, this molecule is an excellent building block to construct highly luminescent materials [9] *via* chemical functionalisation. In 1,10-phenanthroline, 2,9- and 4,7-positions are highly susceptible towards nucleophilic attack, while positions 5,6- or 3,8- with higher electronic densities are preferred by electrophilic reagents [10]. Therefore, the synthesis of various phenanthroline-based materials can be carefully planned to manipulate their electronic structure by controlling the substitution pattern. However, phenanthroline molecules often suffer from low solubility in most (organic) solvents due to the efficient π-π stacking [11].

In our earlier work, we showed that the substitution of 5,6-positions with an imidazolyl unit can provide a good synthetic strategy to develop various phenanthroline-based probes for imaging [4,5]. In this study, the first two objectives were (i) to improve solubility through incorporating bulky lipophilic chains, which limit intermolecular interactions that lead to unwanted π-π stacking, and (ii) to improve the emission efficiency *via* structural changes which tune the energies of π-π* and n-π* electronic levels. Usually, n-π* transitions are deactivated *via* non-radiative processes, causing a low quantum yield. In this context, the substitution of hydrogen *H*-(N) with an aromatic group in imidazolyl could alter the electronic distribution, leading to changes in electronic spectra. Additionally, we aimed (iii) to understand how the incorporation of branches into the phenanthroline structure alters their pH response, and (iv) to exploit their potential as chelating agents (Fig. 1).

* Corresponding author. School of Design, University of Leeds, Leeds, LS2 9JT, UK
E-mail address: n.sergeeva@leeds.ac.uk (N.N. Sergeeva).

https://doi.org/10.1016/j.dyepig.2023.111844
Received 15 August 2023; Received in revised form 24 November 2023; Accepted 24 November 2023
Available online 3 December 2023

To assess the latter in the phenanthroline compounds, we tested their applicability as ligands in heteroleptic $[Ir(C^{\wedge}N)_2(N^{\wedge}N)]^+$ complexes. Iridium complexes were investigated because iridium compounds display rich photophysical behaviour, which is exploited in photocatalysis [12], biology and medicine [13–17], photosensitisers [6,18,19], and light-emitting materials [20,21].

2. Materials and methods

All reagents were used without further purification, unless otherwise stated. All reactions were carried out under a nitrogen atmosphere and were stirred with a magnetic stirrer, unless otherwise stated. ESI supporting document contains the procedure for the synthesis of compounds **1**,**4-10**, and corresponding NMR data for all starting materials and products: **Phen1-5** and **Ir1-5**, descriptions of spectrophotometric data including TFA dilution experiments, fluorescence measurements e.g. quantum yields, and modelling data.

2.1. Computational analysis

Density functional theory calculations were carried out using Gaussian16 software [22] with the B3LYP functional [23] and 6-31G(d) basis set. Geometries of all molecules were fully optimised. Molecular orbitals were visualised using VESTA [24]. Absorption calculations of **Phen1-5** and protonated **Phen2-5** in the gas phase were carried out using time-dependent density functional theory (TDDFT), again using the B3LYP functional and 6-31G(d) basis set, by considering 100 excitations for **Phen1-4** and 120 excitations for **Phen5**. Excitations of **Phen1** and **Phen5** with oscillator strengths above 0.1 in the region 250–500 nm were analysed. Emission transitions were calculated using geometries optimised for the first excited states. Dihedral angle analysis of **Phen3** and **Phen5** was carried out by scanning the dihedral angle N═C−C═C between phenanthroline and phenylene in steps of 10° and relaxing all the other coordinates, starting from the optimised energy minima, both in the ground and in the first excited state of the molecules.

2.2. Synthesis and characterisation

2.2.1. 2-{4-[(2-octyldodecyl)oxy]phenyl}-1H-imidazo[4,5-f][1,10]phenanthroline (Phen1)

A mixture of 1,10-phenanthroline-5,6-dione (988 mg, 4.66 mmol), 4-[(2-octyldodecyl)oxy]benzaldehyde (1.7 g, 4.2 mmol) and ammonium acetate (6.5 g, 84.6 mmol) in glacial acetic acid (28 mL) was refluxed under nitrogen for 24 h. The reaction mixture was poured into water and treated with ammonia solution (35 %) until neutral pH was reached. The precipitate was filtered off and washed with water. The solid was dissolved in DCM and the resulted organic layer was washed with water and dried over $MgSO_4$. The solvents were evaporated under reduced pressure. The residue was purified by column chromatography on silica gel (gradient eluent: DCM-EtOH, 10:1 to pure EtOH) yielding the target compound as a yellow solid (560 mg, 22%). ^{1}H NMR (400 MHz, $CDCl_3$) δ ppm 8.87 (s, 2H), 8.75 (s, 2H), 8.27 (d, J = 8.5 Hz, 2H), 7.35 (s, 2H), 6.76 (d, J = 8.5 Hz, 2H), 3.72 (d, J = 5.3 Hz, 2H), 1.69 (s, 1H), 1.22 (s, 36H), 0.84 (m, 6H); ^{13}C NMR (100 MHz, $CDCl_3$) δ ppm 160.7, 152.6, 147.2, 143.8, 130.9, 128.5, 123.3, 122.8, 114.8, 71.1, 38.0, 32.0, 32.0, 31.4, 30.1, 29.8, 29.7, 29.7, 29.5, 29.4, 26.9, 22.8, 22.8, 14.2; *m/z* (ES+): Found: 593.4227 [M+H], requires: 593.4214; FTIR (ν max/cm^{-1}): 3072, 2920, 1610, 1579, 1525, 1483, 1455, 1401, 1360, 1333, 1291, 1246 cm^{-1}; M.p. >350 °C.

2.2.2. 2-{3,4-bis[(2-octyldodecyl)oxy]phenyl}-1H-imidazo[4,5-f][1,10]phenanthroline (Phen2)

The synthesis follows the procedure described for **Phen1**: 1,10-phenanthroline-5,6-dione (0.75 g, 3.54 mmol), 3,4-bis[(2-octyldodecyl)oxy]benzaldehyde (1.7 g, 2.4 mmol) and ammonium acetate (3.6 g, 47.2 mmol) in glacial acetic acid (20 mL). **Phen2** as an orange solid (227 mg, 15 %). ^{1}H NMR (400 MHz, $CDCl_3$+TFA) δ ppm 9.32 (d, J = 8.2 Hz, 2H), 9.03 (d, J = 4.7 Hz, 2H), 7.94 (dd, J = 8.2, 4.7 Hz, 2H), 7.73 (d, J = 8.5 Hz, 1H), 7.65 (s, 1H), 6.90 (d, J = 8.5 Hz, 1H), 3.94 (d, J = 4.8 Hz, 2H), 1.96–1.75 (m, 1H), 1.59–1.11 (m, 34H), 0.99–0.71 (m, 12H); ^{13}C NMR (100 MHz, $CDCl_3$+TFA) δ ppm 155.1, 152.0, 150.6, 146.6, 136.5, 135.6, 126.4, 125.8, 122.3, 119.9, 119.8, 116.9, 114.1, 113.1, 112.7, 111.2, 110.8, 72.2, 72.0, 38.4, 38.2, 32.1, 31.4, 30.3, 29.9, 29.9, 29.9, 29.8, 29.8, 29.6, 29.6, 27.1, 22.9, 14.2; *m/z* (ES+): Found: 889.7298 [M+H], requires: 889.7293; FTIR (ν max/cm^{-1}): 3084, 2954, 2920, 2851, 1605, 1564, 1522, 1489, 1394, 1260, 1218, 1133, 1068, 1029, 806, 739; M.p. 85–87 °C.

2.2.3. 2-{4-[(2-octyldodecyl)oxy]phenyl}-1-phenyl-1H-imidazo[4,5-f][1,10]phenanthroline (Phen3)

The synthesis follows the procedure described for **Phen1**: 1,10-phenanthroline-5,6-dione (1.5 g, 6.9 mmol), 4-[(2-octyldodecyl)oxy]benzaldehyde (2.30 g, 5.7 mmol), aniline (0.63 mL, 6.9 mmol) and ammonium acetate (4.40 g, 57.1 mmol) in glacial acetic acid (25 mL). **Phen3** as a brown solid (3.1 g, 81 %). ^{1}H NMR (400 MHz, $CDCl_3$) δ ppm 9.19 (dd, J = 4.4, 1.7 Hz, 1H), 9.14 (dd, J = 8.1, 1.7 Hz, 1H), 9.04 (dd, J = 4.3, 1.5 Hz, 1H), 7.75 (dd, J = 8.1, 4.4 Hz, 1H), 7.65 (dt, J = 8.9, 4.4 Hz, 3H), 7.54 (dd, J = 7.9, 1.6 Hz, 2H), 7.50 (d, J = 8.9 Hz, 2H), 7.43 (dd, J = 8.4, 1.5 Hz, 1H), 7.28 (dd, J = 8.4, 4.3 Hz, 1H), 6.82 (d, J = 8.9 Hz, 2H), 3.81 (d, J = 5.8 Hz, 2H), 1.75 (dd, J = 11.5, 5.8 Hz, 1H), 1.26 (s, 38H), 0.88 (t, J = 6.7 Hz, 6H); ^{13}C NMR (100 MHz, $CDCl_3$) δ ppm 160.4, 152.5, 149.1, 147.9, 145.0, 144.5, 138.4, 136.3, 130.8, 130.7, 130.3, 129.0, 128.0, 126.9, 124.2, 123.6, 122.2, 122.1, 120.0, 114.6, 71.2, 38.0, 32.1, 31.5, 30.2, 29.8, 29.7, 29.5, 27.0, 22.8, 14.3; *m/z* (ES+): Found: 670.4534 [M+H], requires: 670.4516; FTIR (ν max/cm^{-1}): 2348, 3064, 2921, 2852, 1686, 1608, 1498, 1465, 1442, 1377, 1296, 1250; M.p. 178–180 °C.

2.2.4. 2-{3,4-bis[(2-octyldodecyl)oxy]phenyl}-1-phenyl-1H-imidazo[4,5-f][1,10]phenanthroline (Phen4)

The synthesis follows the procedure described for **Phen1**: 1,10-phenanthroline-5,6-dione (685 mg, 3.2 mmol), 3,4-bis[(2-octyldodecyl)oxy]benzaldehyde (2.3 g, 3.2 mmol), aniline (0.35 mL, 3.8 mmol) and ammonium acetate (2.49 g, 32.2 mmol) in glacial acetic acid (14 mL). **Phen4** as a red crystalline-glue (1.50 g, 48%). ^{1}H NMR (400 MHz, $CDCl_3$) δ ppm 9.16 (m, 2H), 9.03 (dd, J = 4.3, 1.5 Hz, 1H), 7.75 (dd, J = 8.1, 4.4 Hz, 1H), 7.70–7.61 (m, 3H), 7.56 (dd, J = 6.5, 3.0 Hz, 2H), 7.44 (dd, J = 8.4, 1.5 Hz, 1H), 7.32–7.27 (m, 1H), 7.16 (dd, J = 8.4, 2.0 Hz, 1H), 7.05 (d, J = 2.0 Hz, 1H), 6.77 (d, J = 8.5 Hz, 1H), 3.83 (d, J = 5.6 Hz, 2H), 3.61 (d, J = 5.6 Hz, 2H), 1.76 (m, 2H), 1.36 (m, 64H), 0.93–0.81 (m, 12H); ^{13}C NMR (100 MHz, $CDCl_3$) δ ppm 152.6, 150.7, 149.2, 148.0, 145.0, 144.6, 138.8, 136.3, 130.8, 130.4, 129.2, 128.1, 126.9, 124.2, 123.7, 122.5, 122.3, 120.1, 114.3, 113.0, 72.0, 71.8, 38.3, 32.2, 31.6, 30.0, 29.9, 29.7, 29.6, 27.2, 22.9, 14.4; *m/z* (ES+): Found: 965.7606 [M+H], requires: 975.7606; FTIR (ν max/cm^{-1}): 3263, 3136, 3054, 2954, 2921, 2852, 1691, 1670, 1599, 1498, 1464, 1443, 1316, 1257, 1223; M.p. 56–58 °C.

2.2.5. 1,4-bis(1-phenyl-1H-imidazo[4,5-f][1,10]phenanthrolin-2-yl)benzene (Phen5)

A mixture of 1,10-phenanthroline-5,6-dione (639 mg, 3.01 mmol), terephthaldehyde (202 mg, 1.51 mmol), aniline (0.28 mL, 3.01 mmol) and ammonium acetate (4.6 g, 60.2 mmol) in glacial acetic acid (4 mL) was refluxed under nitrogen for 24 h. The reaction mixture was then cooled to room temperature before the amount of glacial acetic acid was reduced under vacuum. The resulting clay was poured into water and neutralised with ammonia solution (35%). The precipitate was obtained using centrifuge and washed with water and diethyl ether. The yellow product was dried using the freeze dryer to give the target compound (0.85 g, 85%). ^{1}H NMR (400 MHz, $CDCl_3$) δ ppm 9.19 (dd, J = 4.3, 1.6 Hz, 2H), 9.11 (dd, J = 8.1, 1.6 Hz, 2H), 9.05 (dd, J = 4.2, 1.5 Hz, 2H), 7.76 (dd, J = 8.1, 4.4 Hz, 2H), 7.72–7.62 (m, 6H), 7.58–7.50 (m, 4H),

7.44 (dd, $J = 8.4$, 1.4 Hz, 2H), 7.30 (dd, $J = 8.4$, 4.3 Hz, 2H); ^{13}C NMR (101 MHz, $CDCl_3$) δ ppm 151.4, 149.3, 148.3, 145.2, 144.7, 137.9, 136.4, 130.9, 130.7, 130.7, 130.6, 129.4, 128.7, 128.2, 127.3, 124.0, 123.7, 122.4, 119.9; *m/z* (ES+): Found: 667.2353 [M+H], requires: 667.2353; FTIR (ν max/cm^{-1}): 3286, 3078, 3056, 1651, 1597, 1564, 1514, 1497, 1465, 1455, 1440, 1425, 1155, 831; M.p. > 350 °C.

2.2.6. Synthesis of μ-dichloro-bridged iridium dimer [Ir(ppy)$_4$Cl$_2$]

A mixture of $IrCl_3$ (202 mg, 0.68 mmol) and 2-phenylpyridine (0.21 mL, 1.49 mmol) in 2-ethoxyethanol and water (3:1) was refluxed at 110 °C overnight. The solid product was filtered off and washed with water, hexane and diethyl ether. The yellow μ-dichloro-bridged Ir dimer was directly used after it was dried under vacuum without further purification (260 mg, 65%). ^{1}H NMR (300 MHz, $CDCl_3$) δ ppm 9.24 (dd, $J = 5.8$, 0.6 Hz, 1H), 7.87 (d, $J = 7.7$ Hz, 1H), 7.73 (td, $J = 7.9$, 1.5 Hz, 1H), 7.48 (dd, $J = 7.6$, 1.0 Hz, 1H), 6.85–6.67 (m, 2H), 6.56 (td, $J = 7.6$, 1.3 Hz, 1H), 5.93 (d, $J = 7.3$ Hz, 1H); *m/z* (ES+): Found: 501.0941 [M/2-Cl], requires: 501.0943.

2.2.7. Compound Ir1

To a solution of **Phen1** (96 mg, 0.16 mmol) in ethanol (40 mL) was added an ethanoic solution of μ-dichloro-bridged Ir dimer (79 mg, 0.07 mmol). The mixture was refluxed for 24 h. Upon cooling, diethyl ether was added, and the reaction mixture was filtered through a sinter funnel. A solid was dried under vacuum, and the target compound was obtained as a bright yellow crystalline solid (150 mg, 86 %). ^{1}H NMR (400 MHz, $CDCl_3$) δ ppm 8.67 (d, $J = 8.3$ Hz, 2H, 9-H), 8.12 (s, 2H), 7.93 (d, $J = 8.1$ Hz, 2H), 7.71 (m, 7H), 7.36 (d, $J = 5.9$ Hz, 2H), 7.03 (m, 7H), 6.84 (t, $J = 6.3$ Hz, 2H), 6.42 (d, $J = 7.5$ Hz, 2H), 3.88 (d, $J = 5.6$ Hz, 2H), 1.87–1.76 (m, 1H), 1.31 (m, 32H), 0.87 (m, 6H); ^{13}C NMR (100 MHz, $CDCl_3$) δ ppm 168.2, 155.1, 150.7, 148.7, 147.9, 143.7, 138.1, 132.0, 130.9, 129.4, 124.9, 123.2, 122.8, 122.0, 119.7, 114.9, 71.1, 38.0, 32.0, 31.5, 30.2, 29.9, 29.7, 29.5, 27.0, 22.8, 14.2; *m/z* (ES+): Found: 1093.5093 [M$^+$], calcd: 1093.5093; FTIR (ν max/cm^{-1}): 3348, 3047, 2920, 2850, 1606, 1583, 1465, 1452, 1362, 1248, 1075, 808, 757, 727.

2.2.8. Compound Ir2

The synthesis follows the procedure described for **Ir1** starting from **Phen2**. Yield: 93 mg, 98%, orange crystalline solid. ^{1}H NMR (400 MHz, $CDCl_3$) δ ppm 8.22 (m, 3H), 7.91 (d, $J = 8.1$ Hz, 2H), 7.70 (m, 6H), 7.37 (s, 2H), 6.99 (m, 8H), 6.40 (d, $J = 7.4$ Hz, 2H), 4.13 (d, $J = 5.3$ Hz, 2H), 3.86 (d, $J = 5.0$ Hz, 2H), 1.84 (s, 4H), 1.27 (m, 64H), 0.86 (m, 12H); ^{13}C NMR (100 MHz, $CDCl_3$) δ ppm 168.2, 155.3, 151.5, 150.6, 149.8, 147.9, 143.7, 138.0, 132.0, 131.0, 124.9, 123.2, 122.8, 121.1, 119.7, 113.2, 112.3, 72.2, 71.8, 38.4, 38.2, 32.1, 31.6, 31.5, 30.3, 29.9, 29.8, 29.6, 29.5, 27.2, 22.8, 14.2; *m/z* (ES+): Found: 1389.8179 [M$^+$], calcd: 1389.8163; FTIR (ν max/cm^{-1}): 3046, 2920, 2851, 1737, 1606, 1477, 1455, 1261, 1062, 809, 758, 728.

2.2.9. Compound Ir3

The synthesis follows the procedure described for **Ir1** starting from **Phen3**. Yield: 42 mg, 98 %, gold crystalline solid. ^{1}H NMR (400 MHz, $CDCl_3$) δ ppm 9.31 (dd, $J = 8.3$, 1.3 Hz, 1H), 8.24 (dd, $J = 5.0$, 1.2 Hz, 1H), 8.14 (dd, $J = 5.0$, 1.2 Hz, 1H), 7.87 (m, 3H), 7.78–7.58 (m, 10H), 7.49 (m, 4H), 7.34 (dd, $J = 31.6$, 5.3 Hz, 2H), 7.12–6.96 (m, 4H), 6.92 (m, 3H), 6.81 (d, $J = 8.9$ Hz, 2H), 6.36 (t, $J = 7.0$ Hz, 2H), 3.79 (d, $J = 5.6$ Hz, 2H), 1.73 (m, 1H), 1.27 (m, 32H), 0.85 (t, $J = 6.7$ Hz, 6H); ^{13}C NMR (100 MHz, $CDCl_3$) δ ppm 168.0, 167.8, 161.1, 155.1, 150.3, 149.9, 149.5, 148.8, 148.7, 148.4, 144.8, 143.8, 143.7, 138.6, 137.2, 137.1, 133.1, 132.0, 131.5, 131.4, 131.3, 131.1, 131.0, 130.9, 130.4, 128.9, 128.5, 127.8, 126.9, 126.7, 126.4, 125.1, 125.0, 123.9, 123.6, 123.0, 122.7, 121.0, 120.2, 120.0, 119.9, 114.8, 71.3, 38.0, 32.1, 32.0, 31.4, 30.1, 29.8, 29.7, 29.5, 27.0, 22.8, 14.3; *m/z* (ES+): Found: 1169.5420 [M$^+$], calcd: 1169.5397; FTIR (ν max/cm^{-1}): 3371, 3046, 2920, 2851, 1680, 1605, 1582, 1562, 1439, 1400, 1248, 1176, 1125, 726, 693.

2.2.10. Compound Ir4

The synthesis follows the procedure described for **Ir1** starting from **Phen4**. Yield: 296 mg, 98%, orange crystalline solid. 1H NMR (400 MHz, CDCl3) δ ppm 9.37 (d, $J = 7.9$ Hz, 1H, 9-H), 8.27 (d, $J = 4.7$ Hz, 1H), 8.18 (s, 1H), 7.97–7.85 (m, 3H), 7.73 (m, 9H), 7.58–7.47 (m, 3H), 7.38–7.29 (m, 1H), 7.17 (d, $J = 8.9$ Hz, 1H), 7.08 (dd, $J = 16.2$, 8.2 Hz, 4H), 7.02–6.92 (m, 3H), 6.78 (d, $J = 8.4$ Hz, 1H), 6.41–6.32 (m, 2H), 3.84 (d, $J = 5.6$ Hz, 2H), 3.59 (d, $J = 5.4$ Hz, 2H), 1.87–1.72 (m, 2H), 1.27 (d, $J = 8.6$ Hz, 64H), 0.97–0.74 (m, 12H); ^{13}C NMR (100 MHz, $CDCl_3$) δ ppm 168.0, 167.8, 155.0, 151.3, 150.1, 149.7, 149.4, 149.2, 148.7, 148.3, 144.8, 144.7, 143.7, 143.6, 138.5, 137.3, 137.1, 131.9, 131.4, 131.2, 133.1, 131.0, 130.2, 128.8, 128.5, 128.4, 127.7, 126.8, 126.6, 126.3, 125.0, 124.9, 123.7, 123.4, 123.1, 122.9, 122.7, 122.5, 120.8, 120.1, 119.9, 119.8, 113.9, 112.7, 71.8, 71.7, 38.1, 32.0, 31.4, 30.2, 29.8, 29.7, 29.5, 29.4, 27.0, 24.7, 22.8, 14.2. m/z (ES+): Found: 1465.8488 [M$^+$], calcd: 1465.8476; FTIR (ν max/cm^{-1}): 3367, 3044, 2920, 2851, 1681, 1605, 1477, 1440, 1259, 1141, 1030, 1007, 757, 725.

2.2.11. Compound Ir5

The synthesis follows the procedure described for **Ir1** starting from **Phen5**. Yield: 60 mg, 27%, brown crystalline solid. ^{1}H NMR (400 MHz, CDCl3) δ ppm 9.31 (dd, $J = 8.2$, 1.2 Hz, 2H), 8.27 (dd, $J = 5.1$, 1.3 Hz, 2H), 8.16 (dd, $J = 5.1$, 1.2 Hz, 2H), 7.96–7.82 (m, 6H), 7.81–7.62 (m, 18H), 7.59 (s, 4H), 7.52 (dd, $J = 8.6$, 5.1 Hz, 4H), 7.41 (d, $J = 5.9$ Hz, 2H), 7.35 (d, $J = 5.9$ Hz, 2H), 7.06 (m, 6H), 6.95 (m, 6H), 6.46–6.30 (m, 4H); *m/z* (ES+): Found: 834.2086 [M/2 + 2], calcd: 834.2083; FTIR (ν max/cm^{-1}): 3323, 3041, 1604, 1581, 1475, 1377, 1157, 756, 720.

3. Results and discussion

3.1. Synthesis of phenanthrolines

Insertion of the lipophilic chains into the phenanthroline core can be potentially achieved by two alternative synthetic routes. The first pathway involves treatment of 1,10-phenanthroline with the oxidant mixture of sodium bromide and concentrated acids (a mixture of H_2SO_4 and HNO_3) leading to 1,10-phenanthroline-5,6-dione **1** (Scheme 1a). A subsequent reaction of **1** with 4-hydroxybenzaldehyde **2** or 2,4-dihydroxybenzaldehyde **3** in the mixture of glacial acetic acid ammonium acetate affords compounds **4** and **5**, respectively. *rac*-9-(Iodomethyl) nonadecane **6** has been synthesised from the corresponding alcohol in the presence of PPh_3, imidazole and iodine with the yield of 93%. Alkylation of **2** with *rac*-9-(iodomethyl)nonadecane affords compound **Phen1**. However, the purification step for **Phen1** has been unsuccessful, and the second synthetic route was undertaken to prepare the target molecules.

Having difficulties with the purification, we developed a new route to synthesise phenanthroline derivatives (Scheme 1b). Compound **6** was used in excess to alkylate aldehyde **2**, producing **7** in the yield of 63%. In the first attempt to synthesise compound **9**, the stoichiometric quantities of the base and iodide **6** were used. However, this led to the formation of **9** in only 15%, and mono alkylated product **8** was isolated in the yield of 29%.

Subsequent variation of reaction conditions showed the optimal molar ratio of base to iodide to be 2:1.8, which produced **9** in the yield of 51%. However, it was not possible to eliminate the side-product **8** due to a steric hindrance caused by a close proximity of *para*- and *meta*-sites for the insertion of the alkyl chains. Condensation of 1,10-phenanthroline-5,6-dione with aldehydes **7** and **8** in the glacial acetic acid with NH_4OAc led to the formation of **Phen1** and **Phen2** in 22 % and 15 % yields, respectively. The observed low yields for both compounds are caused by their amphiphilic nature and the ease of protonation leading to solubility issues in aqueous and organic solvents, which limits their straightforward isolation. The synthesis of compounds **Phen3** and **Phen4** bearing *Ph*-N group at the imidazolyl unit was carried out in one-step by refluxing of an appropriate aldehyde **7** or **9** with **1** in the presence of

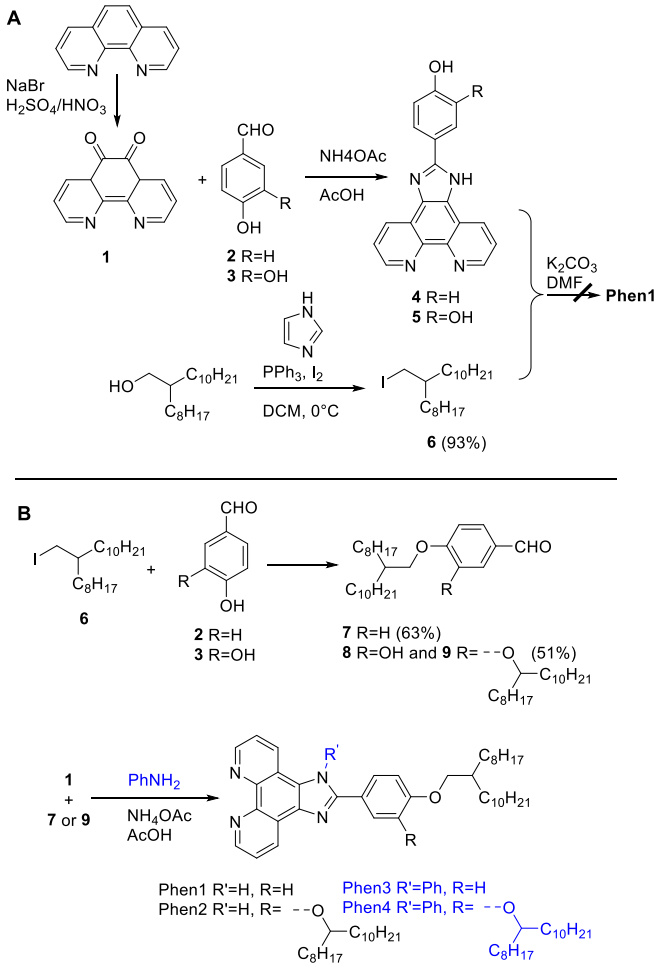

Scheme 1. (a) Route 1: Attempted synthetic route to **Phen1**. (b) Route 2: Successful synthetic pathway to **Phen1-4**.

aniline. To overcome purification difficulties, which plagued the final yield for **Phen1** and **Phen2**, an optimisation of the reaction conditions for **Phen3** was undertaken. The optimal ratio of the reagents for dione: **8**: aniline was 1.3 : 1.0: 1.2 equivalents, respectively; this ratio led to 81% yield of the product. Although the same ratio of dione: **9**: aniline (1.0 : 1.0: 1.2 eq) was used to produce **Phen4**, the yield of the target molecule was only 48%. This is due to the side-reaction leading to the aniline-adduct. In contrast, a highly hydrophobic **Phen5** was synthesised through the condensation of 1,10-phenanthroline-5,6-dion **1**, aniline, terephthaldehyde and ammonium acetate in glacial acetic acid under reflux with the excellent yield of 85 % (Scheme 2).

3.2. Photophysical properties

Photophysical characterisation was carried out to understand the effect of *N*-substitution and the presence of a lipophilic chain on the optical properties of the materials (see Fig. 1). Absorption behaviour of the individual compounds in DCM is recorded in Fig. 2. The spectra of

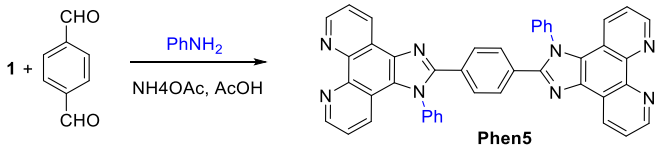

Scheme 2. Synthetic route to compound **Phen5**.

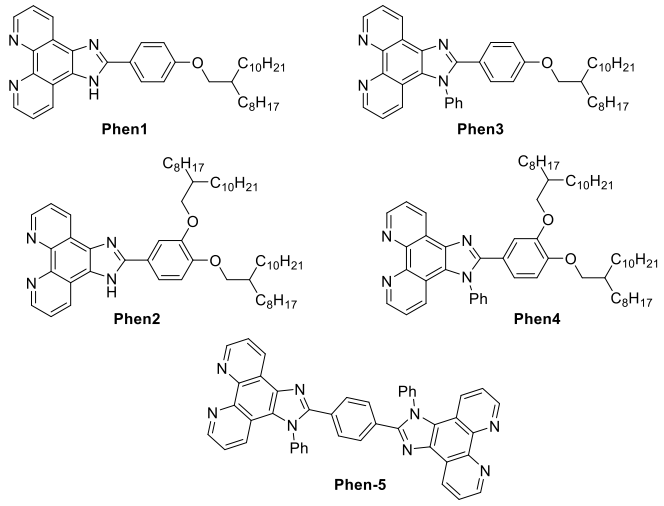

Fig. 1. Structures of the lead compounds Phen1-5.

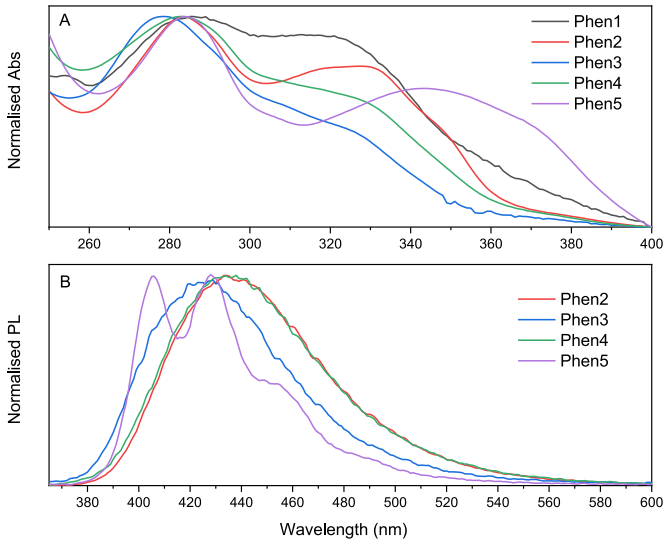

Fig. 2. (a) UV–vis absorption and (b) emission (λ_{ex} 350 nm) spectra of **Phen1-5** in DCM.

Phen1-5 display similarities in the UV-blue region, indicating that the 2-phenyl-1*H*-imidazo-phenanthroline core is a dominant feature between 275 and 285 nm. Comparing **Phen1-4**, we observed a reduction of molar absorptivity for the red-shifted absorption band ($\lambda_{max} > 300$ nm), which is the result of substituting *H*-(N) to *Ph*-(N) in the imidazolyl unit (Fig. 2, Table 2).

Computational analysis of absorption. The calculated absorption spectra for **Phen1-5** (Fig. 3a) show very good agreement with the experiment. The shape of the absorption bands and the difference between **Phen1-4** and **Phen5** can be explained by the molecular orbitals (MOs) involved in the absorption transitions (Fig. 3, Table 1). In **Phen1** (considered as a representative example of **Phen1-4** containing one phenanthroline unit) the excitations involve orbitals spread across the whole molecule, as illustrated in Fig. 3b for the first intense transition from HOMO to the LUMO and LUMO+1.

In **Phen5**, the first transition at 374 nm is from the HOMO to the LUMO, where both orbitals are spread over the whole **Phen5** molecule (Fig. 3c), i.e. over more atoms than in **Phen1**. Thus, the size of the conjugated region in **Phen5** is much larger than in **Phen1**, therefore, the first excitation for **Phen5** is at a longer wavelength than for **Phen1**.

Table 1
Principal excitations (absorption) and the corresponding transitions of **Phen1** and **Phen5** in the region 250–500 nm.

	Excitations (absorption)	Transitions
Phen1	329.51 nm, f = 0.4848	HOMO → LUMO (42%), HOMO → LUMO+1 (49%)
	303.83 nm, f = 0.3463	HOMO → LUMO+2 (84%)
	276.45 nm, f = 0.3146	HOMO-1→ LUMO+1 (35%), HOMO → LUMO+3 (36%)
	267.52 nm, f = 0.2082	HOMO-1→ LUMO (40%), HOMO-1 → LUMO+1 (20%), HOMO-3 → LUMO+1 (17%)
Phen5	374.32 nm, f = 1.4154	HOMO → LUMO (98%)
	291.21 nm, f = 0.1363	HOMO-2→LUMO (49%), HOMO-1→LUMO+1 (36%)
	263.13 nm, f = 0.2684	HOMO-3→LUMO+3 (42%)
	261.14 nm, f = 0.4685	HOMO-3→LUMO+1 (10%), HOMO-2→LUMO+2 (30%)
	254.63 nm, f = 0.1123	HOMO-3→LUMO+6 (32%), HOMO-2→LUMO+5 (36%)
	250.72 nm, f = 0.1573	HOMO-9→LUMO (25%) HOMO-8→LUMO (16%)

Table 2
UV–vis absorption and photoluminescence (PL) data for compounds **Phen1-5** in DCM.

	Absorption		PL	
	λ_{max} nm	ε $M^{-1}cm^{-1}$	λ_{PL} nm	Φ_{PL} %
Phen1[a]	286	1800	n.a.	n.a.
	332	1300		
Phen2	283	37,000	437	20
	328	29,000		
Phen3	278	33,000	426	20
	308[b]	19,000		
Phen4	282	33,000	437	19
	327[b]	20,000		
Phen5	284	35,000	404, 427,453[b]	68
	341	34,000		

[a] Poor response due to low solubility of **Phen1** in DCM.
[b] Shoulder band.

The next set of excitations in **Phen5** in the region 250–292 nm involves lower-lying occupied orbitals and higher-lying unoccupied orbitals, which are not delocalised over the whole molecule but are localised on its phenanthroline rings, i.e. on a smaller area than the HOMOs and LUMOs in **Phen1** (see MO plots in Fig. 3d). The phenylene group in the middle breaks the conjugation of the MOs (HOMO-2 and below, LUMO+1 and above) of **Phen5** into two separate regions. Because of this break in conjugation, the second excitation and higher excitations of **Phen5** occur at significantly shorter wavelengths than the first excitations, resulting in the double peak in the absorption spectrum of **Phen5.**

Photoluminescence (PL). Photophysical properties of 1,10-phenanthroline have been extensively studied, and phenanthroline itself has a very negligible emission (Φ = 0.87 %) [25] in DCM. Studies suggested that phenanthroline and phenanthrene have very similar absorption spectra, and therefore the lowest energy band can be assigned to allowed-spin transitions π-π* [26,27]. Although the emission mainly originates from π-π* transitions, phenanthroline has closely lying π-π* and n-π* levels. Deactivation *via* non-radiative pathways is usually observed in n-π* transitions, which are involved in the singlet state deactivation causing a small quantum yield. Consequently, a promising strategy to improve the emission is to increase the energy gap between those two states.

Several approaches are available to increase the energy gap and to obtain a wide range of highly luminescent compounds with emission bands from UV to NIR. This includes functionalisation at various ring positions, complexation with transition metals and lanthanides or protonation of the phenanthroline nitrogen atoms [26]. In particular, the latter is a fruitful but not widely exploited strategy [25,28], which was investigated in this work. Our effort to improve the quantum yield by extending π-conjugation of the phenanthroline core was successful. The fluorescence quantum yield was calculated according to the literature method using anthracene and 9,10-diphenyl anthracene as cross-references [29]. Although modification of the aromatic system of phenanthroline in 5,6-positions is not a common strategy, it turned out to be effective in improving the quantum yield (Table 2).

Additionally, by linking two aromatic moieties in **Phen5**, an impressive quantum yield of 68% is achieved. Notably, all compounds show large Stokes shifts, which is a requirement in fluorescence imaging of biomaterials.

TDDFT calculations showed that the principal transitions responsible for the emission of **Phen1-4** are the transitions between the LUMO+1 and the HOMO at the wavelengths of 338–348 nm, i.e. at longer wavelengths than absorption, with high predicted oscillator strengths of 0.44–0.48. For **Phen5**, the principal transition was between the LUMO and the HOMO, at a longer wavelength of 440 nm with a much higher

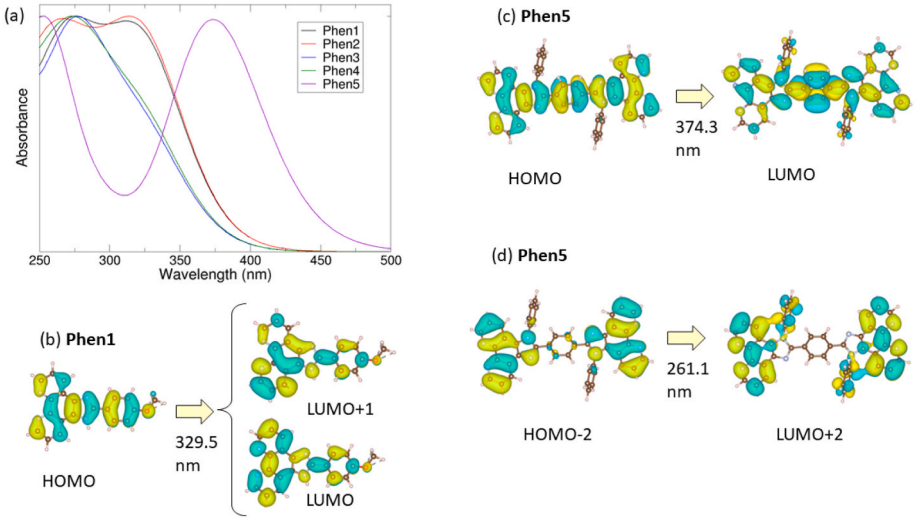

Fig. 3. (a) Calculated UV–vis absorption spectra of **Phen1-5**, (b) molecular orbitals involved in the first strong excitation of **Phen1** at 329.5 nm, (c) molecular orbitals involved in the first strong excitation of **Phen5** at 374.3 nm, (d) molecular orbitals involved in the second strong excitation of **Phen5** at 261.1 nm.

oscillator strength of 1.94.

Computational analysis of vibrational freedom. Analysis of vibrational freedom by investigating the rotation around the dihedral angle between phenanthroline and phenylene can provide a tentative explanation for the difference in PL properties between **Phen5** and **Phen1-4**. Our calculations show that in the molecules without side phenyl groups (**Phen1-2**), both the ground state and the first excited state are planar, therefore the PL transition would proceed directly from the excited state minimum to the ground state minimum with no restriction to vibrational freedom. In **Phen3** and **4** (**Phen3** energies as a function of the dihedral angle shown in Fig. 4), the excited state is planar, the ground state is non-planar, but the planar geometry is only 0.019 eV above the minimum (below kT = 0.025 eV at room temperature), therefore the molecule can easily access both ground state minima at −30° and +30°, passing through the maximum at 0°. In **Phen5** (energy profile also shown in Fig. 4), the excited state is also planar, the ground state is non-planar, the planar geometry is also only 0.02 eV above the minimum. However, there are two slightly different minima at ± 30°, so the deeper minimum will be preferred, and this is likely to result in some restriction to vibrational freedom. This is because the two Ph side groups prefer to be far apart from each other (this is also why the **Phen5** minima at 150° and 210° are less stable, because they involve a greater steric clash of the Ph side groups than the minima at ± 30°). The highest rotational barrier is also larger for **Phen5** than **Phen3** both in the ground state (0.17 eV vs 0.14 eV) and in the excited state (0.55 eV vs 0.44 eV), making it more difficult for **Phen5** to access the minima at +150° and +210° and further restricting its rotational freedom and resulting in fewer different available PL transitions.

It can be concluded that **Phen5** has several slightly different minima in the ground state. It is likely that emission transitions from the excited state conformation that is similar to the lowest ground state minimum are preferred, while for **Phen3** and the rest of the series there is no strong preference for particular conformations, and emission can occur from any excited state conformation close to the ground state minimum.

3.3. Acidochromism

Acidochromism has important applications in chemistry and biology, especially around the development of optical probes and sensors [30]. The spectrophotometric analysis of **Phen1-5** upon gradual addition of trifluoroacetic acid (TFA, 0.25 eq aliquots) was performed in DCM (Fig. 5). As expected, all compounds exhibit acidochromic behaviour in the presence of an acid (Fig. SI S2.1-S2.5). Although the absorption intensity of all bands in **Phen1** changed upon the addition of TFA, an improvement in the solubility of the compound in the acidic environment was thought to be the main reason rather than an exclusive response to the protonation. Thus, this compound was left out from the further analysis. In **Phen1-5**, the protonation can occur at two key sites, namely, phenanthroline-*N* [1] or benzimidazole-*N* [31] atoms. Furthermore, this series presents two different benzimidazole-*N* sites: **Phen2** and **Phen3-4** are examples of imidazolyl unsubstituted (*H*-N) and substituted (*Ph*-N) sites, respectively. However, **Phen2-4** exhibit similar acidochromic behaviour. Non-protonated **Phen2** shows a strong structured absorption band in the UV region at λ_{max} 283 nm (Table 2, Fig. 2a), but upon the addition of TFA, significant spectral changes are observed. A new absorption band with the maximum at λ_{max} 320 nm assigned to the protonated form emerges, and after the addition of 1.0 equivalent of acid, no further spectral changes are observed (Fig. SI S2.1-S2.5).

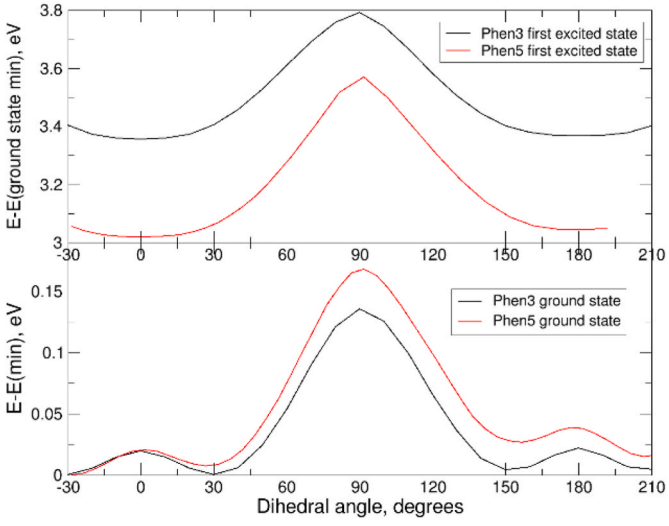

Fig. 4. Dependence of the ground and excited states' energies on the dihedral angle for the analysis of vibrational freedom of **Phen1-5**. The horizontal axis is the dihedral angle between phenanthroline and phenylene.

This is supported by a linear trend of *y*(absorption) = *f*(concentration) between 0 and 1.0 equivalents of TFA. This red-shift of the absorption peak on the addition of TFA displays a positive acidochromism [32]. The red shift suggests extension of conjugation [33] in these molecules. Overall, the responses in **Phen2-4** are very similar; these results suggest that protonation of **Phen2-4** occurs at the same site, therefore *Phen*-N, which is available in all the molecules, is the preferable protonation site. Although *imidazolyl*-N is available in **Phen2**, only mono protonation takes place, suggesting a limited participation of the latter site. Our DFT calculations confirm that protonation at the phenanthroline-*N* site is more favourable by 0.46–0.59 eV for all of these molecules. Similarly, **Phen5** shows a gradual increase of the 302 nm band and a decrease of the 284 nm band upon addition of TFA until after 2.0 eq of TFA (0–4.0 eq) are added. TDDFT calculations of optical absorption spectra of **Phen2-5** (Fig. 3d) confirm that protonation broadens these molecules' absorption, consistent with the experimental observations.

When looking at the response to the presence of acid in these systems using fluorescence, we should consider a possibility of inversion between the strongly emissive π-π* state and the poorly emissive n-π* state. Protonation can particularly stabilise the n-π* state relative to the π-π* state and therefore decrease the emission [34]. Therefore, we can expect a noticeable change in the emission response. Indeed, fluorescence is completely quenched upon gradual addition of TFA for all compounds **Phen1-5** (Fig. 5b,c and S2.1-2.5). Overall, **Phen2-4** show similar behaviour, with **Phen2** slightly overperforming **Phen3** and **Phen4**, suggesting a limited benefit of a second protonation site, as a strong response is only observed between 0 and 1.0 eq of TFA with a weaker response after that. Similarly, **Phen5** shows rapid quenching of emission; this continues up until 2.0 eq of TFA are added. Although further addition of TFA leads to further reduction in the fluorescence intensity, it is significantly less dramatic.

3.4. Synthesis of heteroleptic Ir(III)-phenanthroline complexes and their photophysical behaviour

The Ir(III) complexes **Ir1-5** were prepared through μ-dichloro-bridged iridium dimer **9**, followed by the cleavage of the dimer in the presence of **Phen1-5** as a N^N ligand (Scheme 3). A big advantage of heteroleptic Ir(III) complexes is that their synthesis generally avoids isomeric contamination, requires mild reaction conditions and supports a wide range of ligands [35]. The complexes **Ir1-4** were isolated in almost quantitative yield of 86–98%; this is likely due to an improved solubility of the ligands due to the presence of the lipophilic chains and their positive impact on the solubility.

Scheme 3 shows an effective way to obtain the binuclear cyclometalated iridium(III) complex **Ir5** by using a bis-N^C-coordinating ligand **Phen5**. The Ir(III) complex was obtained in a yield of 27% by the direct reaction of the μ-dichloro-bridged iridium dimer in dry ethanol in the presence of the ligand (N^N) **Phen5** in the ratio 1.5:1. In

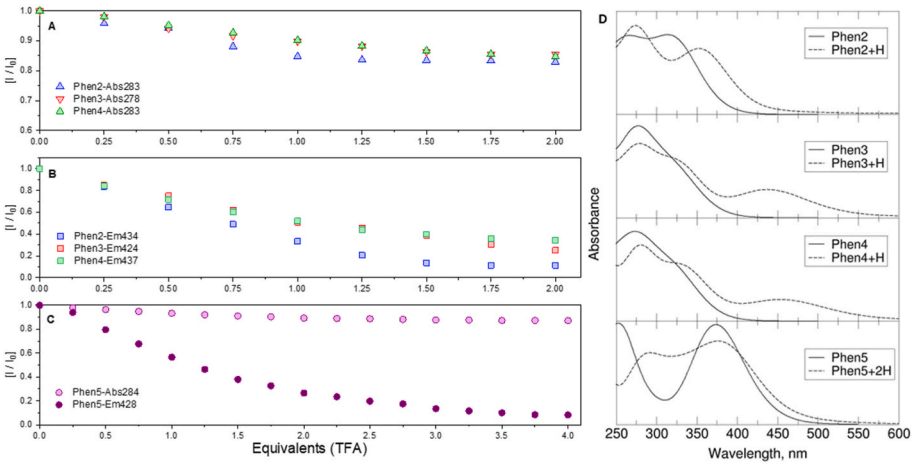

Fig. 5. Spectrophotometric titration of **Phen2-5** with TFA (0.25 eq aliquots) in DCM: (a) UV-Absorption response for **Phen2-4**; (b) Emission response for **Phen2-4** (wavelength of excitation is 350 nm); (c) UV-Absorption and emission response for **Phen5** (wavelength of excitation is 350 nm); (d) Calculated optical absorption spectra of non-protonated *Phen*-N and protonated *Phen*-NH $^{+}$ species for **Phen2-5**.

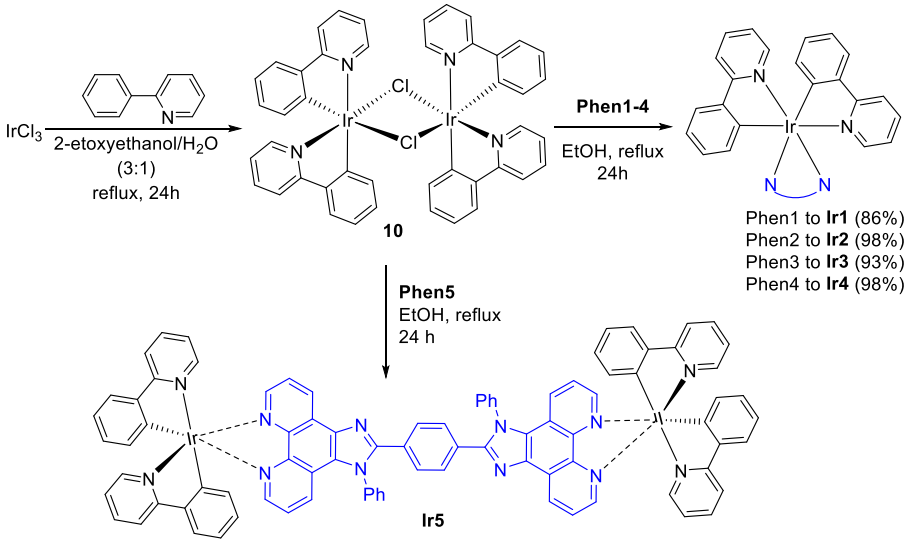

Scheme 3. Synthesis of mononuclear Ir(III) complexes **Ir1-4** and **Ir5.**

contrast to **Ir1-4**, such low yield is likely due to a lower solubility of the free ligand as well as its bidental nature leading to alternative products e.g. mono complexes. Moreover, due to the presence of the lipophilic ligands, these materials appear to be highly viscous oils-solids.

3.5. Photophysical properties

The optical properties of the five cationic iridium(III) complexes were studied in dichloromethane. The absorption spectra shown in Fig. 6a reveal that **Ir1-5** complexes intensely absorb in the ultraviolet region between 250 nm and 350 nm, which can be associated with π-π* and n-π* transitions of **Phen1-5** and 2-phenylpyridinyl ligands. Although the absorption spectra of compounds **Ir1-5** display similarities to the free **Phen1-5** ligands in this region, the iridium complexes show additional absorption bands in the UV–visible region (330–510 nm), which can be assigned to metal-ligand charge transfer (MLCT) transitions [36–38]. The bands between 350 and 450 nm are typically assigned to ^{1}MLCT, whereas a weaker shoulder that appears at a longer wavelength (450–510 nm) is typically associated with ^{3}MLCT [39]. These changes indicate successful formation of the complexes and efficient interactions between ligands and metal centre.

Fluorescence in this type of organometallic systems is negligible or absent as a result of spin-orbit coupling between the metal and the ligand, which accelerates the intersystem crossing to the triplet state [40]. Emission in these systems arises from ^{3}MLCT or a mixture of ^{3}MLCT and ^{3}LC transitions [41]. Photoluminescence spectra of complexes **Ir1-5** in DCM (Fig. 6b, Table 3) show broad, featureless bands with a maximum intensity in the range of 539–571 nm upon excitation with the light at 350 nm.

Diversifying structure of the ligands can significantly affect luminescence properties; in our case, extension of the π-conjugation decreases the band gap [42], producing a bathochromic shift in the emission spectra. The yellow emission observed for **Ir1-5** can be assigned to MLCT transitions, which are typically associated with phosphorescence from ^{3}MLCT [43–45]. Large Stokes shifts (220–290 nm) are observed for the **Ir1-5** complexes, even larger than for the free **Phen1-5**, making them interesting targets for imaging and photosensitisation applications. The quantum yield of photoluminescence (Φ_{PL}) was calculated by cross-reference method and the data are summarised in Table 3. Commonly, a low Φ_{PL} is observed for the iridium complexes; nevertheless, compounds **Ir1-5** produce fairly high Φ_{PL} yields of 3–7 %.

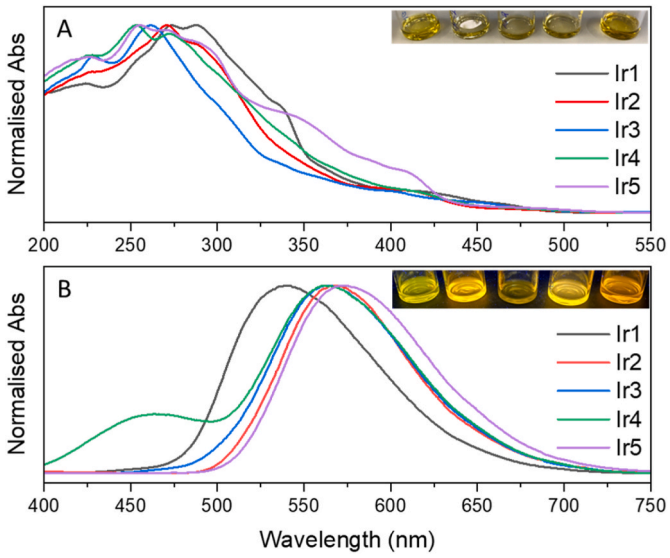

Fig. 6. Normalised spectra of **Ir1-5** in DCM: (a) UV–vis absorption (Abs); (b) photoluminescence (PL) collected when excited at λ_{ex} 350 nm. Images of **Ir1-5** solutions (in the order 1 → 5): (a) under ambient light; (b) under UV light (350 nm).

Table 3
UV–vis Absorption and emission data for compounds **Ir1-5** in DCM.

	Absorption	Emission	
	λ_{max} nm	λ_{PL} nm	Φ_{PL} %
Ir1	273, 288, 414[a]	539	7.0
Ir2	255, 272, 340, 415[a], 470[a]	567	6.0
Ir3	271, 287, 415[a]	564	3.0
Ir4	254, 272, 415[a]	460[a], 564	5.4
Ir5	255, 270, 296, 348, 412[a], 469[a]	571	5.4

[a] Shoulder band.

Despite the complexity of the ligands, the emission characteristics for **Ir1-5** are similar across the board because the photoluminescent properties are governed by the transitions defined by the ligands and the energy is mainly determined by a "global" LUMO energy represented by the ligands [40,46,47].

4. Conclusion

Phenanthroline based ligands **Phen1-4** bearing lipophilic aliphatic chains have been synthesised in 3 steps. Also, **Phen 5** was prepared to provide a template for a binuclear iridium complex. The structure-property relationship was studied by UV–vis and fluorescence spectroscopy revealing that the absorption and photoluminescence properties strongly depend on the derivatisation of the phenanthroline core. Computational analysis explains the difference in the absorption behaviour observed in **Phen5**, with the lowest-energy transition between the HOMO and LUMO which are delocalised across the whole molecule, while the higher energy transitions are between HOMO-1, -2 etc. and LUMO+1, +2 etc. which are localised on phenanthrolines and are spatially separated into two halves by the central phenylene. Quantum yields of **Phen2-4** have significantly improved compared to unmodified 1,10-phenanthroline. Moreover, bidental **Phen5** has proven to be the most effective in emission. The response of **Phen2-5** derivatives to acid was studied spectrophotometrically, revealing that protonation induces stabilisation of the electronic transitions with a positive acidochromism (red-shift). The synthesis of mononuclear iridium (III) complexes **Phen2-4** has afforded the target compounds in the excellent yield of 86–98% due to the presence of lipophilic ligands; these materials appear to be highly viscous oils. The optical properties of these complexes are similar across the series as they are strongly influenced by the nature of the phenanthroline core. Furthermore, the compounds exhibited a strong yellow emission at 539–571 nm and large Stokes shift (220–290 nm) is observed for the series. The PL quantum yields were calculated using the cross-reference method and were in the range of 3–7%.

CRediT authorship contribution statement

Ana M. Garrote Cañas: Formal analysis, Investigation, Methodology, Validation. **Xue Yong:** Formal analysis, Methodology, Validation. **Maha S. Alenezi:** Formal analysis, Investigation, Validation. **Natalia Martsinovich:** Investigation, Methodology, Supervision, Validation, Writing – original draft, Writing – review & editing. **Natalia N. Sergeeva:** Conceptualization, Methodology, Supervision, Validation, Writing – original draft, Writing – review & editing.

Declaration of competing interest

The authors declare that they have no known competing financial interests or personal relationships that could have appeared to influence the work reported in this paper.

Data availability

No data was used for the research described in the article.

Acknowledgements

This research was supported in part through the Clothworkers' Foundation Fund and the University of Leeds. N.M. and X.Y. acknowledge the use of the Sol computer cluster at the Department of Chemistry, University of Sheffield. N.M. and X.Y. are thankful to NERC (grant no. NE/T010924/1), and X.Y. thanks The Leverhulme Trust for the Early Career Fellowship.

Appendix A. Supplementary data

Supplementary data to this article can be found online at https://doi.org/10.1016/j.dyepig.2023.111844.

References

[1] Bencini A, Lippolis V. 1,10-Phenanthroline: a versatile building block for the construction of ligands forvarious purposes. Coord Chem Rev 2010;254:2096–180.
[2] Zhong H-J, Wang W, Kang T-S, Yan H, Yang Y, Xu L, Wang Y, Ma D-L, Leung C-H. A rhodium(III) complex as an inhibitor of neural precursor cell expressed, developmentally down-regulated 8-activating enzyme with in vivo activity against inflammatory bowel disease. J Med Chem 2017;60(1):497–503.
[3] Qiu K, Liu Y, Huang H, Liu C, Zhu H, Chen Y, Ji L, Chao H. Biscylometalated iridium(III) complexes target mitochondria or lysosomes by regulating the lipophilicity of the main ligands. Dalton Trans 2016;45:16144–7.
[4] Sergeeva NN, Donnier-Marechal M, Vaz GM, Davies AM, Senge MO. Simple but powerful: phenanthroline-based small molecules for cellular imaging and cancer screening. Bioorg Med Chem Lett 2011;21:4385–8.
[5] Sergeeva NN, Donnier-Marechal M, Vaz G, Davies AM, Senge MO. Synthesis and evaluation of the europium(III) and zinc(II) complexes as luminescent bioprobes in high content cell-imaging analysis. J Inorg Biochem 2011;105(12):1589–95.
[6] Lu Y, McGoldrick N, Murphy F, Twamley B, Cui X, Delaney C, Máille GMÓ, Wang J, Zhao J, Draper SM. Highly efficient triplet photosensitizers: a systematic approach to the application of Ir(III) complexes containing extended phenanthrolines. Chem Eur J 2016;22:11349–56.
[7] Liu J, Chen Y, Li G, Zhang P, Jin C, Zeng L, Ji L, Chao H. Ruthenium(II) polypyridyl complexes as mitochondria-targeted two-photon photodynamic anticancer agents. Biomaterials 2015;56:140–53.
[8] Chen T, Liu Y, Zheng W-J, Liu J, Wong Y-S. Ruthenium polypyridyl complexes that induce mitochondria-mediated apoptosis in cancer cells. Inorg Chem 2010;49(14):6366–8.

[9] Kuo C-J, Li T-Y, Lien C-C, Liu C-H, Wu F-I, Huang M-J. Bis(phenanthroimidazolyl) biphenyl derivatives as saturated blue emitters for electroluminescent devices. J Mater Chem 2009;19:1865–71.
[10] Alreja P, Kaur N. Recent advances in 1,10-phenanthroline ligands for chemosensing of cations and anions. RSC Adv 2016;6:23169–217.
[11] Zhao Qiang, Liu Shujuan, Shi Mei, Li Fuyou, Jing Hao, Tao Yi, Huang Chunhui. Tuning photophysical and electrochemical properties of cationic iridium(III) complex salts with imidazolyl substituents by proton and anions. Organometallics 2007;26:5922–30.
[12] Prier CK, Rankic DA, MacMillan DWC. Visible light photoredox catalysis with transition metal complexes: applications in organic synthesis. Chem Rev 2013;113 (7):5322–63.
[13] Ma D-L, Chan DS-H, Leung C-H. Group 9 organometallic compounds for therapeutic and bioanalytical applications. Accounts Chem Res 2014;47(12): 3614–31.
[14] Ko C-N, Li G, Leung C-H, Ma D-L. Dual function luminescent transition metal complexes for cancer theranostics: the combination of diagnosis and therapy. Coord Chem Rev 2019;381:79–103.
[15] Soldevila-Barreda JJ, Metzler-Nolte N. Intracellular catalysis with selected metal complexes and metallic nanoparticles: advances toward the development of catalytic metallodrugs. Chem Rev 2019;119(2):829–69.
[16] Lo KK-W. Luminescent rhenium(I) and iridium(III) polypyridine complexes as biological probes, imaging reagents, and photocytotoxic agents. Accounts Chem Res 2015;48(12):2985–95.
[17] Mondal A, Shanavas S, Sen U, Das U, Roy N, Bose B, Paira P. Mitochondria-targeted half-sandwich iridium(iii)-Cp*-arylimidazophenanthroline complexes as antiproliferative and bioimaging agents against triple negative breast cancer cells MDA-MB-468. RSC Adv 2022;12(19):11953–66.
[18] Zhao J, Wu W, Sun J, Guo S. Triplet photosensitizers: from molecular design to applications. Chem Soc Rev 2013;42(12):5323–51.
[19] Xu Y, Wang X, Song K, Du J, Liu J, Miao Y, Li Y. BSA-encapsulated cyclometalated iridium complexes as nano-photosensitizers for photodynamic therapy of tumor cells. RSC Adv 2021;11(25):15323–31.
[20] Housecroft CE, Constable EC. Over the LEC rainbow: colour and stability tuning of cyclometallated iridium(III) complexes in light-emitting electrochemical cells. Coord Chem Rev 2017;350:155–77.
[21] Ch. 26-34, Porphyrin handbook vol.4.
[22] Gaussian 16, Revision C.01, M.J. Frisch et al., Gaussian, Inc., Wallingford CT, 2016, https://gaussian.com/citation/.
[23] Becke AD. Density-functional thermochemistry. III. The role of exact exchange. J Chem Phys 1993;98:5648–53.
[24] Momma K, Izumi F. VESTA 3 for three-dimensional visualization of crystal, volumetric and morphology data. J. Appl. Crystallogr. 2011;44:1272–6.
[25] Accorsi G, Listorti A, Yoosaf K, Armaroli N. 1,10-Phenanthrolines: versatile building blocks for luminescent molecules. materials and metal complexes 2009; 38:1690–700.
[26] Markovitsi D, Bengs H, Ringsdorf H. Charge-transfer absorption in doped columnar liquid crystals. 1992. p. 553–6.
[27] Henry MS, Hoffman MZ. Photophysics and photochemistry of aromatic nitrogen heterocycles. Fluorescence from 2,2'-bipyridine and 1,10-phenanthroline 1979;83: 618–25.
[28] Accorsi G, Listorti A, Yoosaf K, Armaroli N. 1,10-Phenanthrolines: versatile building blocks for luminescent molecules, materials and metal complexes. Chem Soc Rev 2009;38:1690–700.
[29] Cañas AMG, Martsinovich N, Sergeeva NN. π-Conjugated indole dyads with strong blue emission made possible by stille cross-coupling and double fischer indole cyclisation. ChemistrySelect 2017;2:2433–8.
[30] Bao L, Jones LO, Garrote Cañas AM, Yan Y, Pask CM, Hardie MJ, Mosquera MA, Schatz GC, Sergeeva NN. Multipurpose made colorimetric materials for amines, pH change and metal ion detection. RSC Adv 2022;12(5):2684–92.
[31] Listorti A, Esposti AD, Kishore RSK, Kalsani V, Schmittel M, Armaroli N. 1,10-Phenanthrolines with tunable luminescence upon protonation: a spectroscopic and computational study. 2007.
[32] Kothavale S, Sekar N. Novel pyrazino-phenanthroline based rigid donor-π-acceptor compounds: a detail study of optical properties, acidochromism, solvatochromism and structure-property relationship. Dyes Pigments 2017;136:31–45.
[33] Singh P, Baheti A, Thomas KRJ. Synthesis and optical properties of acidochromic amine-substituted benzo[a]phenazines. J Org Chem 2011;76(15):6134–45.
[34] Pina F, Bernardo MA, García-España E. Fluorescent chemosensors containing polyamine receptors. Eur J Inorg Chem 2000;2000(10):2143–57.
[35] You Y, Nam W. Photofunctional triplet excited states of cyclometalated Ir(III) complexes. beyond electroluminescence 2012;41:7061–84.
[36] Tsuboi T, Aljaroudi N. Transient photoluminescent response with three decay lifetimes of phosphorescent organic molecule Ir(ppy)3 doped in polycarbonate. Opt Mater 2005;27(12):1859–63.
[37] Lamansky S, Djurovich P, Murphy D, Abdel-Razzaq F, Lee H-E, Adachi C, Burrows PE, Forrest SR, Thompson ME. Highly phosphorescent bis-cyclometalated iridium complexes: synthesis, photophysical characterization, and use in organic light emitting diodes. J Am Chem Soc 2001;123(18):4304–12.
[38] Schreier MR, Guo X, Pfund B, Okamoto Y, Ward TR, Kerzig C, Wenger OS. Water-soluble tris(cyclometalated) iridium(III) complexes for aqueous electron and energy transfer photochemistry. Accounts Chem Res 2022;55(9):1290–300.
[39] Wang H, Liao Q, Fu H, Zeng Y, Jiang Z, Ma J, Yao J. Ir(ppy)3 phosphorescent microrods and nanowires: promising micro-phosphors. J Mater Chem 2009;19(1): 89–96.
[40] Demas JN, DeGraff BA. Applications of luminescent transition platinum group metal complexes to sensor technology and molecular probes. Coord Chem Rev 2001;211(1):317–51.
[41] Reddy MLP, Bejoymohandas KS. Evolution of 2, 3′-bipyridine class of cyclometalating ligands as efficient phosphorescent iridium(III) emitters for applications in organic light emitting diodes. J Photochem Photobiol C Photochem Rev 2016;29:29–47.
[42] Skórka Ł, Filapek M, Zur L, Małecki JG, Pisarski W, Olejnik M, Danikiewicz W, Krompiec S. Highly phosphorescent cyclometalated iridium(III) complexes for optoelectronic applications: fine tuning of the emission wavelength through ancillary ligands. J Phys Chem C 2016;120(13):7284–94.
[43] Matsushita T, Asada T, Koseki S. Relativistic study on emission mechanism in tris (2-phenylpyridine)iridium. J Phys Chem C 2007;111(18):6897–903.
[44] Goushi K, Kawamura Y, Sasabe H, Adachi C. Unusual phosphorescence characteristics of Ir(ppy)3 in a solid matrix at low temperatures. Jpn J Appl Phys 2004;43:L937.
[45] Stampor W, Mężyk J. Electromodulation of photoluminescence in vacuum-evaporated films of fac-tris(2-phenylpyridine)iridium(III). Chem Phys 2007;337 (1):151–60.
[46] Nazeeruddin MK, Humphry-Baker R, Berner D, Rivier S, Zuppiroli L, Graetzel M. Highly phosphorescence iridium complexes and their application in organic light-emitting devices. J Am Chem Soc 2003;125(29):8790–7.
[47] Li J, Djurovich PI, Alleyne BD, Yousufuddin M, Ho NN, Thomas JC, Peters JC, Bau R, Thompson ME. Synthetic control of excited-state properties in cyclometalated Ir(III) complexes using ancillary ligands. Inorg Chem 2005;44(6): 1713–27.